AEROSPACE REPORT NO.
ATR-2018-00052

Adjoint Monte Carlo Simulations and Improved Sector Shielding Calculations with Geant4

January 9, 2018

Mark D. Looper
Magnetospheric and Heliospheric Sciences
Space Sciences Department

Prepared for:

Senior Vice President, Engineering and Technology Group

Authorized by: Engineering and Technology Group

Acknowledgments

The author acknowledges many useful discussions with T. Paul O'Brien on the use, and particularly the normalization, of Monte Carlo simulation results. This work was supported by the Aerospace Technical Investment Program (ATIP) under a Long Term Capability Development (LTCD) project, JO 6416-01.

Abstract

The adjoint Monte Carlo simulation technique can be used to greatly speed calculation of radiation dose or other quantities related to a small sensitive volume, like an electronic part, inside a much larger inert shielding volume, like a spacecraft. For several years the Geant4 open-source Monte Carlo radiation-transport toolkit has included the capability to perform such simulations as well as more conventional forward simulations; we document here how to use this capability, qualitatively and quantitatively, and compare results of adjoint and forward Monte Carlo simulations in a simple test geometry. We find that the two methods agree well for an external radiation environment consisting of electrons, but that results from the adjoint technique are a factor of 2x to 3x too high for protons that have low enough energies to come to a stop, or nearly so, in the sensitive target. We discuss an extension of techniques already in use to combine different forward Monte Carlo simulations, in order to use a focused forward simulation to supersede results in the suspect part of the parameter space for a global adjoint simulation. We also have developed an improvement on the even faster, albeit less physically detailed, sector shielding technique to improve its accuracy as a substitute for adjoint Monte Carlo simulations of protons.

Contents

Figures

1. Forward and Adjoint Monte Carlo Simulations

Geant4 [1] is an open-source toolkit to enable a user to simulate the transport of energetic-particle radiation through matter. It is very detailed, modeling the trajectories of individual particles through a user-defined geometry with user-chosen physics lists that can simulate a wide variety of electromagnetic or nuclear interactions. It is also very general, providing access to all properties (position, velocity, charge, energy deposit, etc.) of each particle at all points along its trajectory, so that the user can tabulate any quantities of interest from simple energy deposit (radiation dose) to complicated sensor backgrounds, production of secondary particles, etc.

The standard use of the code is to implement "forward" Monte Carlo simulations, wherein the trajectories of individual particles are modeled with such non-deterministic processes as nuclear interactions, scattering, energy-loss fluctuations, etc., being sampled randomly from the relevant probability distribution functions. With many simulated particles the ensemble exhibits realistic behavior, including rare occurrences like production of certain secondary particles, large-angle scattering, etc., that would not be captured in a tabulation of average particle behavior. See, e.g., Looper et al. [3].

This thoroughness, however, comes at a high computational cost; we routinely run simulations on hundreds of cluster cores for days at a time. For some problems, a full forward Monte Carlo simulation with good statistics may simply be prohibitive. For example, consider a situation as in Figure 1, where we need to tabulate the energy (radiation dose) deposited in a small sensitive target, say an electronic part, that is part of a much larger geometry, say an entire satellite. A complete forward Monte Carlo Simulation would require simulating particles from the external radiation environment that are incident over the entire surface of the larger volume, arriving at each surface point from all directions in the locally outward-facing hemisphere. One cannot simply model the particles that start out "aimed" at the target, like those labeled "A", even though this would be a much more manageable subset of the incident particles since one could omit particles like those with trajectories labeled "B" that never encounter the target. However, this would also miss particles that have trajectories like that labeled "C", which start out aimed away from the target but then have an interaction such as scattering, production of secondary particles, etc., that cause either the original particle or its secondaries to affect the target. Such trajectories will constitute a small fraction of the trajectories that start out looking like those labeled "B", but their contribution may be important if the sensitive part is deep inside shielding or under other circumstances.

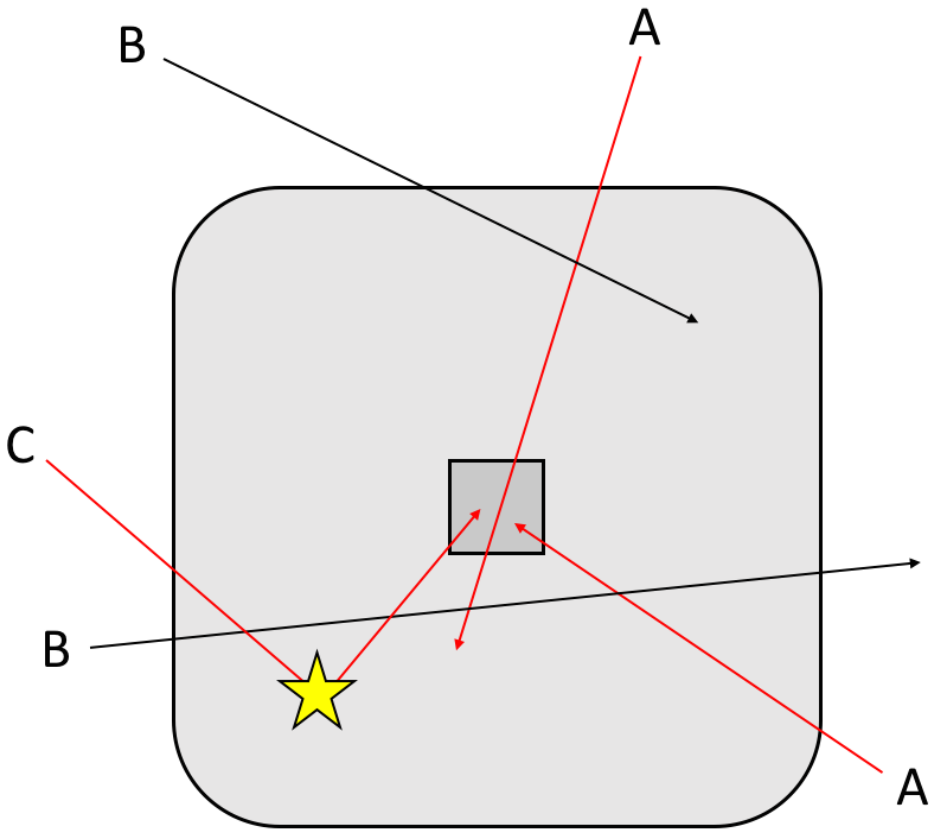

Figure 1. Schematic of radiation exposure of a small sensitive volume or part (dark gray) within a larger volume of shielding like a spacecraft (light gray). Labels on particle trajectories (arrows) are discussed in the main text.

As an alternative to illuminating the entire surface of the enclosing volume with primary particles (typically protons or electrons in the space environment), a "reverse" or "adjoint" Monte Carlo simulation starts with particles at or near the sensitive target, and then traces them probabilistically backward in time to find external primary particles at the surface of the large volume that could, with some probability that is tabulated trajectory by trajectory, have caused the initially-simulated particle to arrive at the target. This backward-in-time simulation can involve particle-species changes, for example with an initial backward

electron that is modeled as having been produced as a secondary delta ray from a proton, which is then traced back to the surface of the simulation volume and identified as a primary particle with some likelihood. Such a simulation has limitations, discussed below, but since every simulated particle intersects the target volume of interest there is no computation time wasted on trajectories like those labeled “B” in Figure 1, and statistics can be built up much faster for quantities of interest like radiation dose.

This capability has been available commercially for a long time, for example in the FASTRAD (www.fastrad.net) and NOVICE (empc.com/novice-software) packages. It has also been introduced and refined within the Geant4 toolkit in the past few years. This report discusses our experience with the Geant4 implementation of the adjoint Monte Carlo technique, comparing its results and how to use them with the results of Geant4 forward simulations in a simple test geometry.

2. How Geant4 Executes an Adjoint Simulation Event

A forward Monte Carlo simulation is conceptually very simple: simulated primary particles are sampled from a source distribution, typically spread isotropically over the outside of the simulated geometry for space applications, and are then transported through the geometry. As they travel, they undergo energy loss, scattering, production of secondaries, and other interactions, and ultimately either come to a stop, decay, or exit the simulation volume. Any secondary particles produced are transported in the same way starting from their origin points, so that there is a very granular modeling of realistic particles illuminating the simulated geometry and proceeding into and through it. One cycle of this process, from the launching of a single primary particle through the disposition of it and of any secondary particles generated as it travels, is an "event" in Geant4 terminology.

An adjoint Monte Carlo simulation involves more steps for each event. First, whereas a forward simulation starts with specific individual primary particles of known species, energy, etc., sampled from the external radiation environment that is being modeled, an adjoint simulation starts with particles which may be penetrating primary particles that reach the target, or secondaries produced by the external primary particles. Thus each adjoint event cycle samples one of each candidate particle species that is to be considered, from a $1/E$ energy spectrum between user-defined upper and lower limits; as of version 10.3 of Geant4, patch level 2 (geant4.10.03.p02) as considered herein, the available choices are electrons, gammas, and protons. (There appear also to be generic ions available, but the example code provided did not make clear how to use them, so they will be ignored hereinafter.) By default only electrons and gammas are considered, and only interactions that transport them or convert one into the other (e.g., bremsstrahlung) are considered; this means that the results can only be applied to an external primary-particle population consisting of electrons and/or gammas. If protons are of interest as external primary particles, then the user can tell the code to launch them as well as part of the adjoint event, and also to consider processes during transport that produce secondary electrons or gammas from primary protons.

Thus for each adjoint event cycle, up to three initial adjoint particles of different species will be launched for transport backward in time. (Geant4 documentation refers to these as "primary" adjoint particles because they are launched at the start of adjoint trajectories, but to avoid confusion with the forward particles that enter the simulation geometry from the outside, we will refer to them as "initial" adjoint particles hereinafter.) Geant4 launches adjoint particles either from the surface of a user-defined physical volume, say a detector chip in a dosimeter, or from the surface of a sphere surrounding the sensitive target or possibly multiple targets. Each adjoint particle is transported backward in time, possibly being transformed in flight into another adjoint species (e.g., an initial adjoint gamma being transformed into an adjoint electron via reverse bremsstrahlung), until the particle being tracked either reaches a user-defined outer boundary that represents the source of the external radiation, or rises above a user-defined upper limit (adjoint particles gain energy as they are transported backward in time) to indicate that an external primary particle would have had to have begun at an energy higher than the range of interest in order to have reached the target along this trajectory. Just as a forward primary particle can spawn multiple secondary particles, so a single initial adjoint particle can experience different adjoint interactions that each represent a possible route by which it might have reached the target; each of these is considered a separate "track" in Geant4, so that a single initial adjoint particle may be associated with multiple candidate external source particles (those that reached the outer simulation boundary), with different probabilistic weights and possibly different species.

For each initial adjoint particle that produces at least one track reaching the outer simulation boundary, a forward-transport step is launched to carry that initial particle forward in time into the target region. Tabulation of energy deposit or other observables occurs just as in a full forward Monte Carlo simulation, so any desired quantity can be logged and associated with an adjoint track (possibly more than one, as

above) with a statistical weight determined by the adjoint transport process. These observables can then be integrated over external-particle populations (energy and angular distributions) of physical interest.

3. Tabulating and Normalizing Results for Forward and Adjoint Simulations

In a typical forward simulation, simulated primary particles to be launched from an outer boundary are sampled from an energy and angular distribution that represents the radiation source to which the geometry being simulated is exposed in the real world. The simulation results are discrete, say a single measurement of energy deposit in a sensitive target for a single simulated primary particle, and so the summed results must be related back to the continuous spectrum from which they were drawn. For simplicity, consider a particle source that is isotropic in direction; then $J = J(E)$ will represent the fluence, in particles per (cm^2 sr MeV), as a function only of particle energy. Let A be the total area of the (convex) illuminated surface in the simulation. Then for any quantity that is a function of energy, say dose per particle $D(E)$ in a sensitive target, the total summed over a range of particle energy will be

$$D_t = \iint D(E)J(E)\cos\theta A dE d\Omega = \pi A \int D(E)J(E)dE \tag{1}$$

(with the cosine factor accounting for particles striking a given patch of the surface obliquely).

Let N_s simulated particles be sampled with a distribution

$$\frac{dN}{dE} = N_s f(E) \tag{2}$$

where $f(E)$ is normalized to integrate to unity over energy between simulation limits E_0 and E_1. For example, if energy is sampled proportionately to $1/E$ within this interval, then

$$f(E) = \frac{1}{E\ln(E_1/E_0)} \tag{3}$$

Using equation 2, equation 1 can be approximated by a sum over simulated particles as

$$D_t \approx \pi A \sum D(E)J(E)\delta E = \sum D(E)J(E)\pi A \frac{\delta N}{N_s f(E)} = \sum wD(E)J(E) \tag{4}$$

where δN is unity for each single simulated particle and

$$w = \frac{\pi A}{N_s f(E)} \tag{5}$$

is the weight, with dimensions of (cm^2 sr MeV), of that simulated particle, $D(E)$ is the simulated value of the observable (say, dose) for that particle, and $J(E)$ is the value of the primary-particle differential fluence spectrum at that particle's energy. If E_0 and E_1 are chosen by pairs from a closely spaced set so that $E_1 = E_0 + \delta E$, then a response function can be calculated by summing over all simulated particles with energies in this range as

$$R(E_0) = \sum_{E\in[E_0,E_1]} \frac{wD(E)}{\delta E} \tag{6}$$

with dimensions rad cm^2 sr if $D(E)$ is dose per particle in rads, for example. This can be convolved in energy with a fluence in particles per (cm^2 sr MeV) to give a total dose, encapsulating the factors multiplying $D(E)$ in equation 1, or with a flux in particles per (cm^2 sr sec MeV) to give a dose rate.

Geant4 handles the scoring of an adjoint Monte Carlo in a very similar way, but with some complications. As noted in section 2, a single initial adjoint particle may produce one or more tracks representing

external particles that could have caused the adjoint particle to have reached the target, each with a different probabilistic weight. This track weight is employed in the same way as w above to model the values of observable quantities; and indeed, if the geometry consists of vacuum outside the target, so that the initial adjoint particle has a probability of unity of having reached the target from the outside of the simulation volume, then the weights reported by the code for tracks representing an unchanged external particle are numerically equal to w in equation 5 with $f(E)$ given by equation 3 (and with A being the area of the adjoint source surface, the outside of either a specific sensitive volume or a sphere around the sensitive volume or volumes, in square mm rather than cm). Thus to calculate the simulated value of an observable quantity, one selects the tracks that represent the external particle of interest (typically either electrons or protons, for space applications) and constructs the sums in equations 4 or 6 from these.

Note that a forward Monte Carlo simulation typically scores observables once for each primary particle event so that, for example, the energy deposit logged in a detector will be the sum of all contributions from the primary particle and from any secondaries, which is how a real detector would respond. (Of course, with the granular information available to the user about all primary and secondary particles, the contribution of each can be teased out separately, but that would not be the typical use case.) An adjoint Monte Carlo simulation, by contrast, considers each particle reaching the target independently, so that there is no way to associate the energy deposit from one particle at the target with that of others that might have been part of the same "shower" (primary particle plus any secondaries) in the real world. This will make no difference if energy deposits due to all external particles are lumped together into a total dose, but if for example (as will be done below in some plots) the observable of interest is not the total energy deposit from all particles but the spectrum of energy deposits from each external primary particle (and all its secondaries), then the energy deposits that would result from the summation of a single shower will be split among multiple adjoint tracks and attributed to separate external primary particles. This is not shown to make much difference in the example geometry discussed below, but if it is of concern then it could be mitigated by choosing the adjoint target surface to be a sphere large enough that showers occurring outside the sphere would be expected to spread out enough that only one secondary particle would interact with the sensitive volume, as in Figure 2. (Showers originating inside the sphere would be tracked using forward physics, and all secondary particles would be correctly associated with a single primary.)

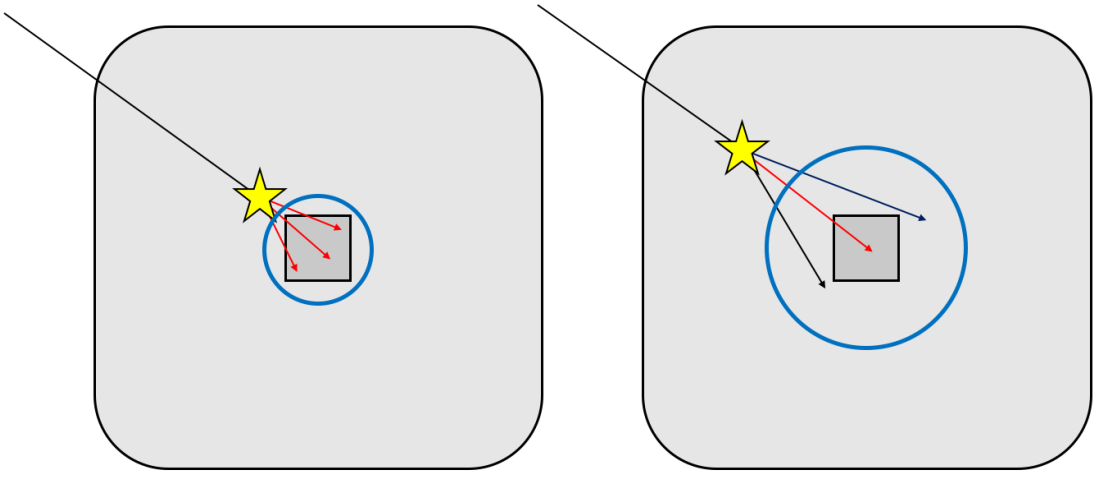

Figure 2. Schematic of different adjoint source surfaces, shown as blue circles representing spheres enclosing the dark gray sensitive volume. Showers occurring outside a larger surface as at right will have fewer secondaries interacting with the sensitive volume (red arrows) per incident particle, and thus fewer instances as at left where different adjoint tracks (separately launched outward and backward in time from the points where the arrows cross the blue circles) are erroneously not associated with a common external primary particle, which might make a difference in some applications.

4. Comparison of Dose Among Various Simulations in a Simple Test Geometry

Figure 3 shows the simple cylindrically symmetric test geometry that will be used for the comparisons in the remainder of this report. Materials (yellow: silicon, blue: aluminum, red: Kovar, gray: Mallory) and thicknesses are representative of the structures around the sensitive chip of a typical microdosimeter (e.g., O'Brien et al. [4]). We only consider one of the two yellow detectors hereinafter; the green circle in the figure shows the size of the spherical adjoint source surface surrounding that detector that we defined, and we will also tabulate particles crossing that spherical surface in the forward simulations.

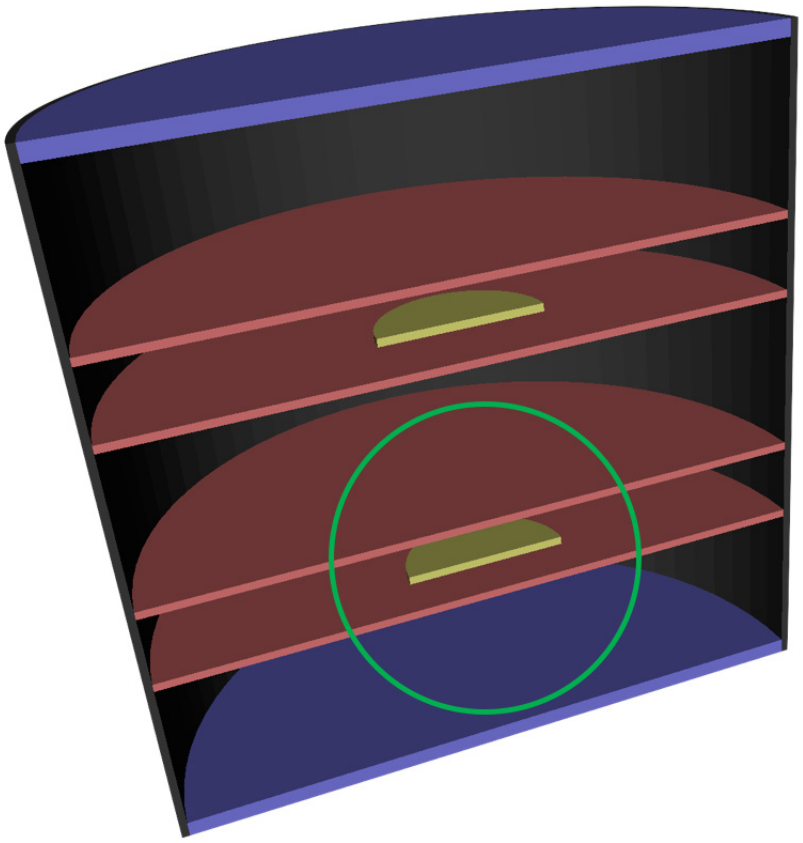

Figure 3. Cross section of cylindrically symmetric Geant4 geometry used for comparisons hereinafter. The yellow detectors are 0.5 cm in diameter and 250 microns thick; only one is considered here. The green circle represents the size and position of the spherical adjoint source around the detector.

Figure 4 shows a first set of results, the dose response from equation 6 for one detector plotted against the energy of primary electrons striking the outside of the geometry. The three curves show results from three different simulations, one adjoint as described in sections 2 and 3 and two forward. The terms in parentheses that are part of the curve labels are two different physics lists: Shielding_EMZ is a "reference physics list" provided as a package as part of the Geant4 code, and ReverseMC01 is the physics list from the example user code provided to show how to perform adjoint simulations. Shielding_EMZ is a very complete compilation of physics models for forward Monte Carlo simulations, with a large variety of nuclear interactions and with electromagnetic physics tuned for the lower energies (compared to particle accelerator energies) of interest in space science and engineering; it is the physics list we currently use for most applications. ReverseMC01 contains both forward and adjoint physics, since as noted in section 2 a complete adjoint simulation includes both forward and reverse transport. The forward physics only includes electromagnetic interactions, with no models of nuclear physics even for protons; this is commensurate with the adjoint physics, which only models reverse electromagnetic processes (as is only reasonable, since adjoint nuclear physics would need to launch a wide variety of additional adjoint particles – neutrons, pions, etc. – in order to trace the range of possible secondaries back to their external primary particles). The blue curve is a standard forward simulation using the forward portion of the ReverseMC01 physics list; the green curve is a full adjoint simulation using both halves of this physics list. As discussed in section 2, for this simulation only gammas and electrons were considered as initial adjoint particles to trace back in time, and energy deposits were only tabulated (with appropriate weights) for tracks that led back to an incident electron at the outer boundary of the geometry.

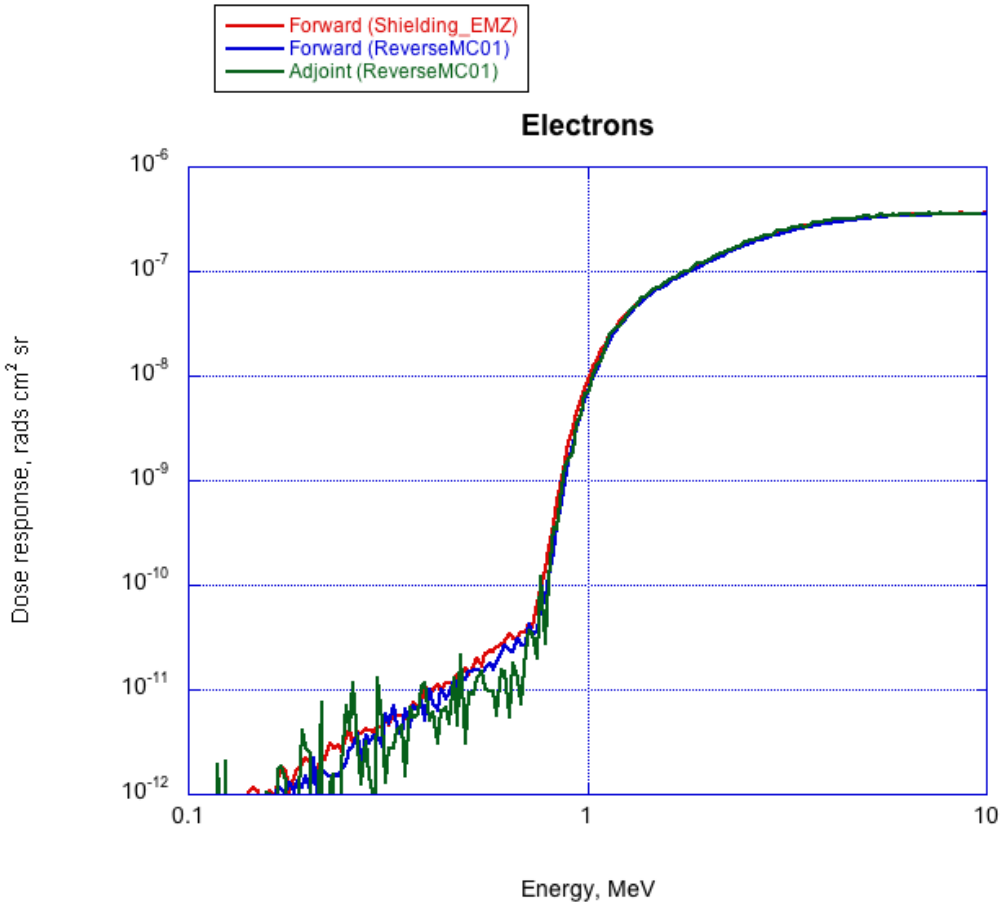

Figure 4. Dose response vs. energy for electrons in one detector of the geometry in Figure 3, for forward simulations with two different physics lists and an adjoint simulation.

One can see that agreement is generally very good between the three cases. The most significant differences are in the subthreshold energy range below about 800 keV, in which electrons are excluded from direct access and some of their energy must be converted to gammas in order to traverse the thickness of shielding. In particular, the statistics are noticeably more ragged for the adjoint simulation; that is because with forward simulations, we can and do boost statistics by running (many) more cases at these low primary energies, whereas in an adjoint simulation any given initial adjoint gamma might come from an external electron primary of any energy and so we cannot selectively boost statistics for the lower external electron energies. However, an adjoint simulation runs much faster than a forward simulation (at least for a more typical case, where the entire geometry is proportionately much larger relative to the sensitive target than is the case in our test setup here), and so it need not be onerous to boost statistics overall in order to pull them up in the subthreshold regime.

Figure 5 shows the same comparison for primary protons striking the outside of the geometry, and here we see some systematic differences between the three simulations. Here the two forward simulations agree very well, except at the highest energies where the Shielding_EMZ physics list starts simulating nuclear interactions, resulting in high-Z fragments that occasionally deposit large pulses of energy in the detector. However, the adjoint simulation results in a noticeably higher dose response below about 100 MeV, up to a factor of 2 or 3 in some places.

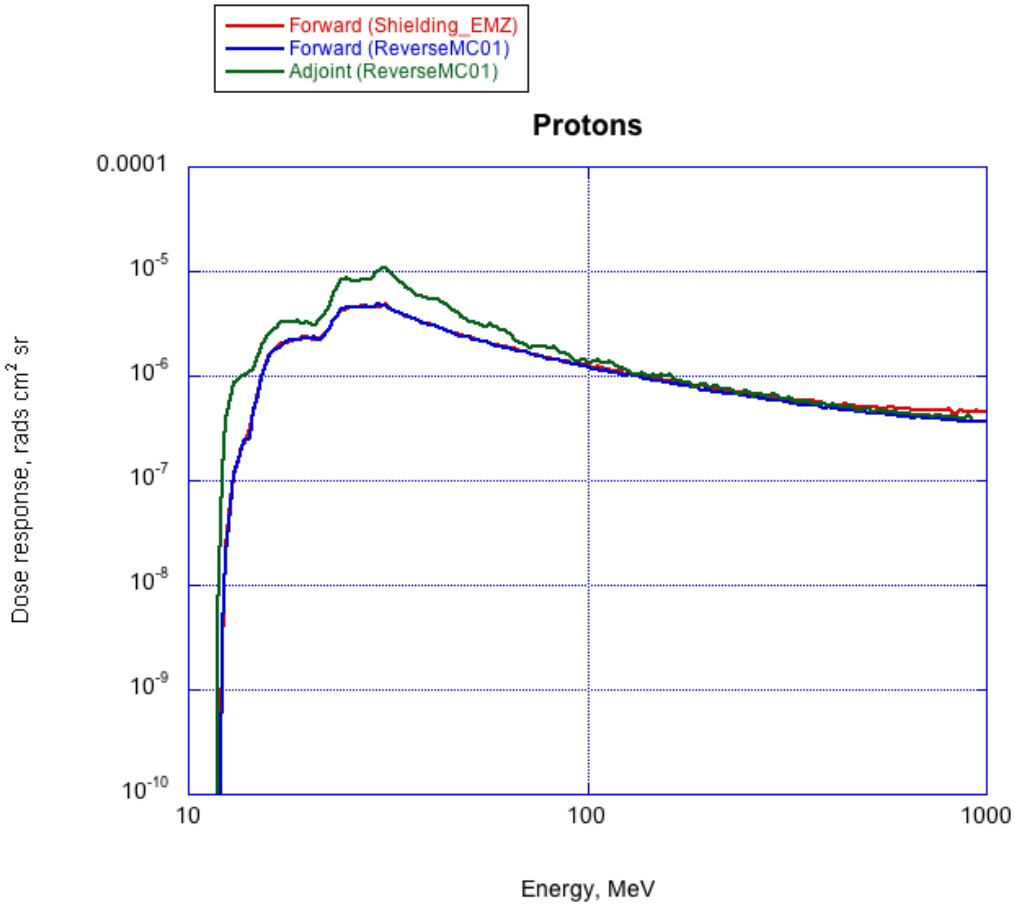

Figure 5. Dose response vs. energy for protons in one detector of the geometry in Figure 3, for forward simulations with two different physics lists and an adjoint simulation.

5. Differences in Adjoint and Forward Simulation Results for Protons

To examine this further, we look at the distribution of energy deposits in the detector for the different simulations. This amounts to replacing $D(E)$ in equation 1 with $d(E, E_{dep})$ giving the differential spectrum of energy deposits E_{dep} at each primary proton energy E. The color bar in the following plots shows the logarithm of this quantity in units of cm^2 sr per MeV (of energy deposit – in Figures 4 and 5 this was divided by the detector's mass to convert it to a dose).

Figure 6 shows the energy deposit spectra produced for each primary proton energy in the forward simulation with the Shielding_EMZ physics list. The coherent streaks at high energy deposits each represent a family of protons coming through a particular subset of the shielding, for example the Mallory enclosure and one Kovar plane, peaking where the energy and angle are just so as to cause the proton to stop in the detector without quite traveling through it and out the other side; events to the left of each peak are protons stopping in the detector (not distinctly visible except where labeled in the figure), and events to the right are protons penetrating the detector. The large red-and white patch toward the bottom is due to knock-on secondary electrons (delta rays) reaching the detector although the primary proton misses it, and the sparse scattering of events to the upper right is due to nuclear interactions each producing a high-Z secondary ion that reaches the detector and deposits a lot of energy. Summing up a vertical strip through this plot and dividing by detector mass would produce a point on the red curve in Figure 5.

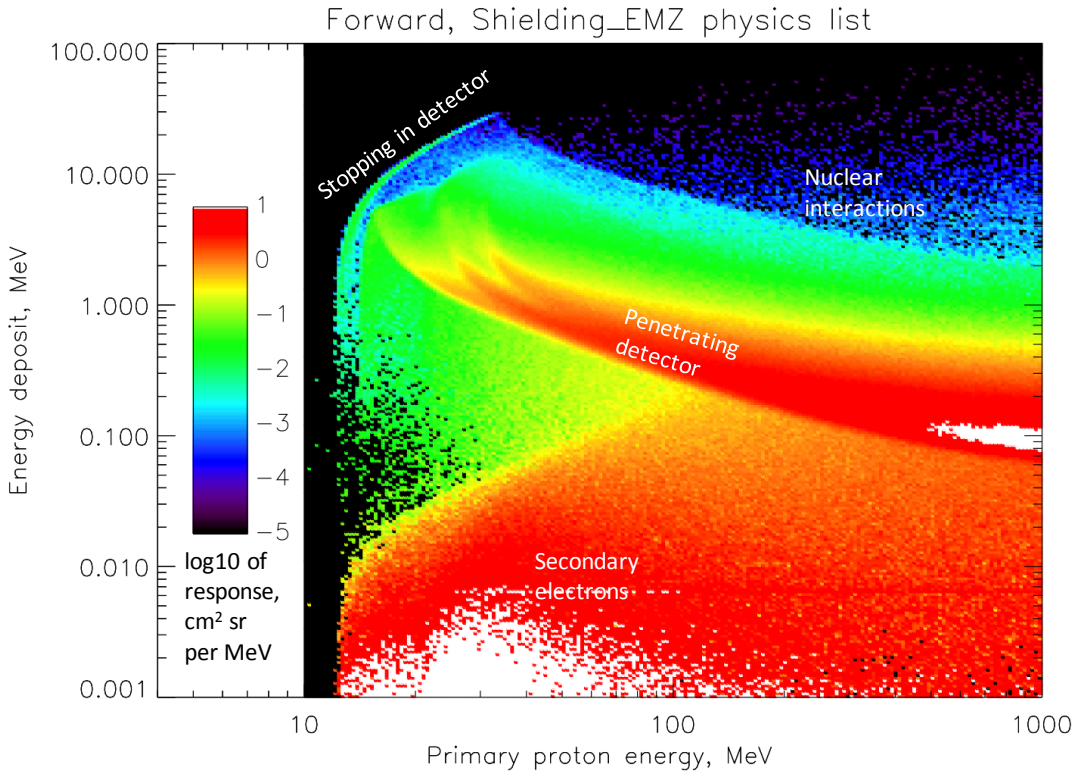

Figure 6. Spectra of energy deposits in detector as a function of primary proton energy, for forward simulation with Shielding_EMZ physics list. Colorscale is logarithm of response in cm^2 sr per MeV of energy deposit.

Figure 7 is the same for the forward simulation with the ReverseMC01 physics list. Consistent with the similarity between the red and blue curves in Figure 5, we see little difference between Figures 6 and 7, except that the latter lacks the large energy deposits at high proton energies (upper right) due to nuclear interactions that are not part of the ReverseMC01 physics list.

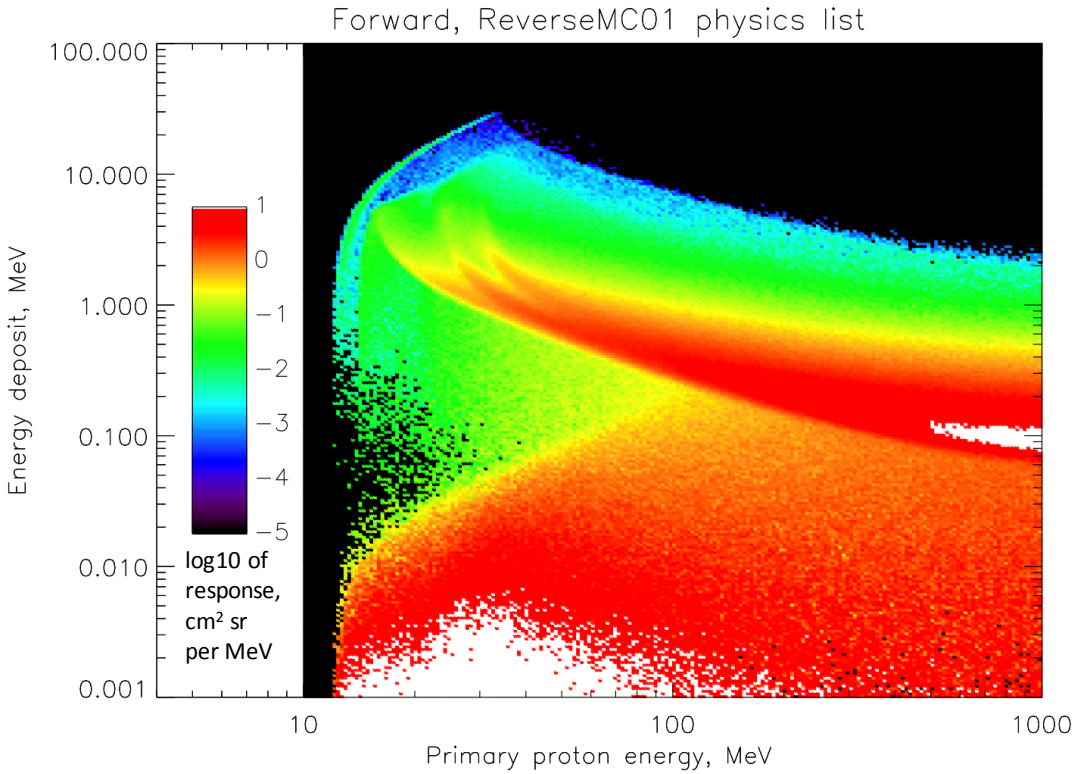

Figure 7. Spectra of energy deposits in detector as a function of primary proton energy, for forward simulation with ReverseMC01 physics list. Same colorscale as Figure 6.

Figure 8 is the same for the adjoint simulation, and here we see a notable intensification of the high-energy-deposit portions of the streaks beginning at about 15 MeV. This suggests that the adjoint physics somehow enhances the weighting of protons that are just about to come to a stop as they reach the detector, relative to the forward case. In addition, we see horizontal streaks at the left of the colored region, around a few hundred keV energy deposit, for which we have not found an explanation. Two known issues with the Geant4 adjoint Monte Carlo code are the separation of secondary-particle energy deposits that would have arisen from a given primary-particle shower from those of each other and of the primary particle as discussed at the end of section 3, and a "rare too high weight" discussed in the documentation for the ReverseMC01 example code. However, the first of these would shift energy deposits downward in this plot, not upward, and the second (1) mostly affects low-energy electrons and gammas, which don't contribute much to proton energy deposits here, and (2) was only flagged in a very few instances during our runs by the diagnostic code we borrowed from the provided ReverseMC01 example. Thus neither of these issues explains the differences seen here between forward and adjoint results.

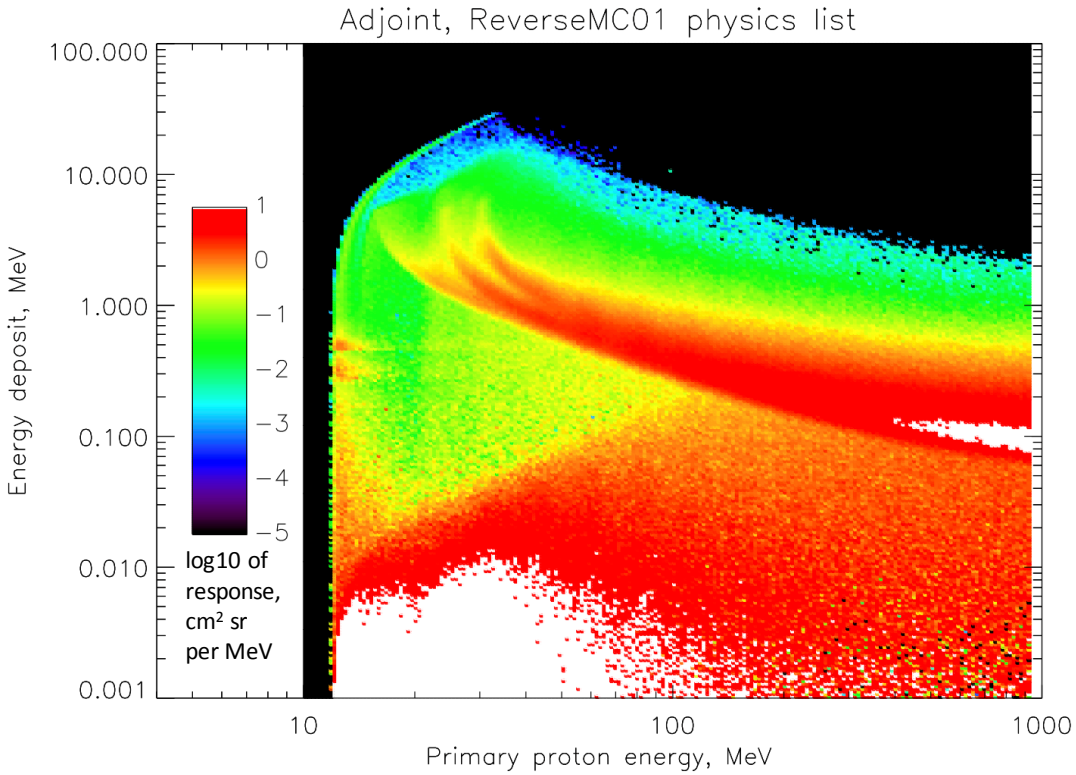

Figure 8. Spectra of energy deposits in detector as a function of primary proton energy, for adjoint simulation with ReverseMC01 physics list. Same colorscale as Figure 6.

Figure 9 is the same kind of plot as Figure 8, but for this simulation the adjoint source was placed on the surface of the detector rather than on a sphere centered on the detector. Statistics are better overall than in Figure 8 because here, when the forward simulation step is done for adjoint particles that were traced back to the external surface, all of the forward particles hit the detector because they are launched inward right from its surface rather than from a sphere around it at some distance. Note that the intensities (colors) match in all of Figures 6–9 for the very highest energy deposits, representing oblique trajectories that have a long pathlength inside the detector; this gives us confidence that the normalization has been done correctly. However, with the larger volume of the simulated geometry being subject to adjoint rather than forward transport in Figure 9 vs. Figure 8, we see that the intensification of the red streaks is greater, and the horizontal bars at hundreds of keV energy deposit are stronger. Also, a pattern of vertical bands with slight intensifications is evident in the range of under 100 to several hundred MeV primary proton energy in both plots, but stronger in Figure 9; we have not determined a reason for this either, but it is subtle enough not to cause much difference between the curves in Figure 5 at these energies (it is slightly visible as ripples in the green curve on either side of 100 MeV).

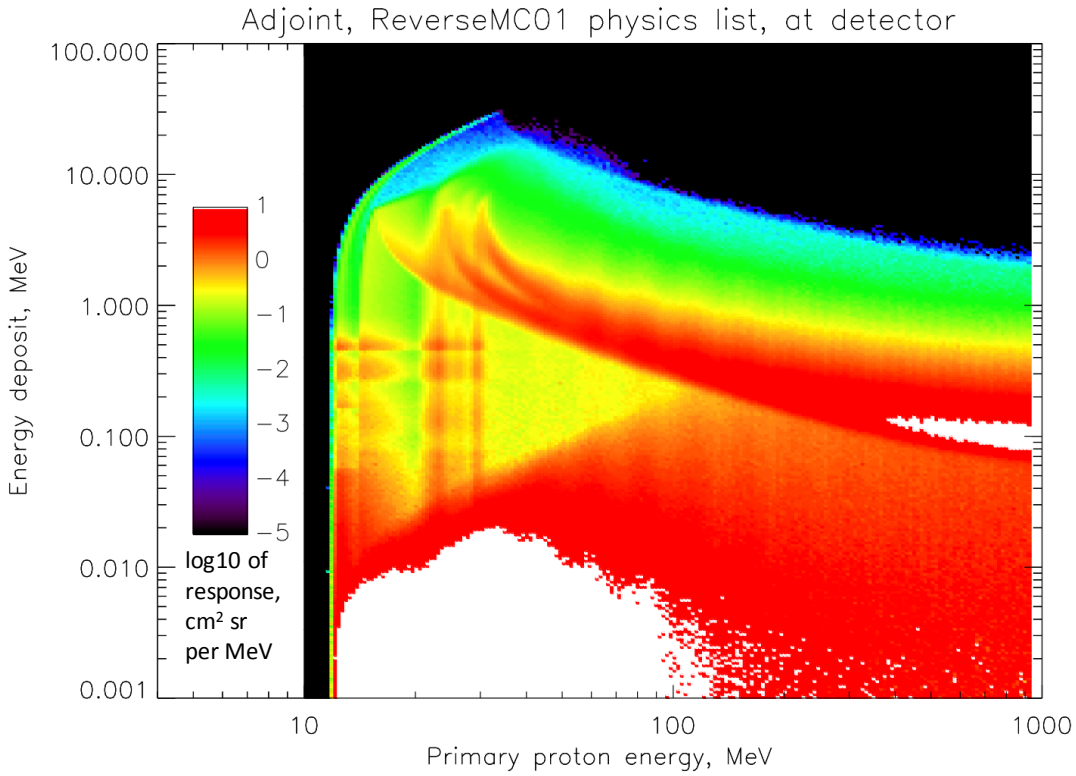

Figure 9. Spectra of energy deposits in detector as a function of primary proton energy, for adjoint simulation with ReverseMC01 physics list and adjoint source placed at the surface of the detector rather than on a sphere around it. Same colorscale as Figure 6.

As mentioned at the end of section 3, it is possible to separate the energy deposits from different species of particles at the target during a forward Monte Carlo simulation, but an adjoint simulation gives us this separation automatically. Figure 10 shows the energy deposit spectra due only to protons reaching the surface of the detector, for the same adjoint simulation as plotted in Figure 9. As noted in the discussion of Figure 6 above, each strong vertical band at primary proton energies of a few tens of MeV is due to a family of protons coming in through a particular combination of inert material and stopping in the detector, so that they deposit whatever energy they have left in the detector. Removing the lower energy deposits due to electrons (prominent in Figures 6–9) and gammas from the plot, we can see that these tracks are quite strong all the way down the Y axis in energy deposit, despite the narrow band of primary proton energies that have just enough range in the inert materials to contribute to each one.

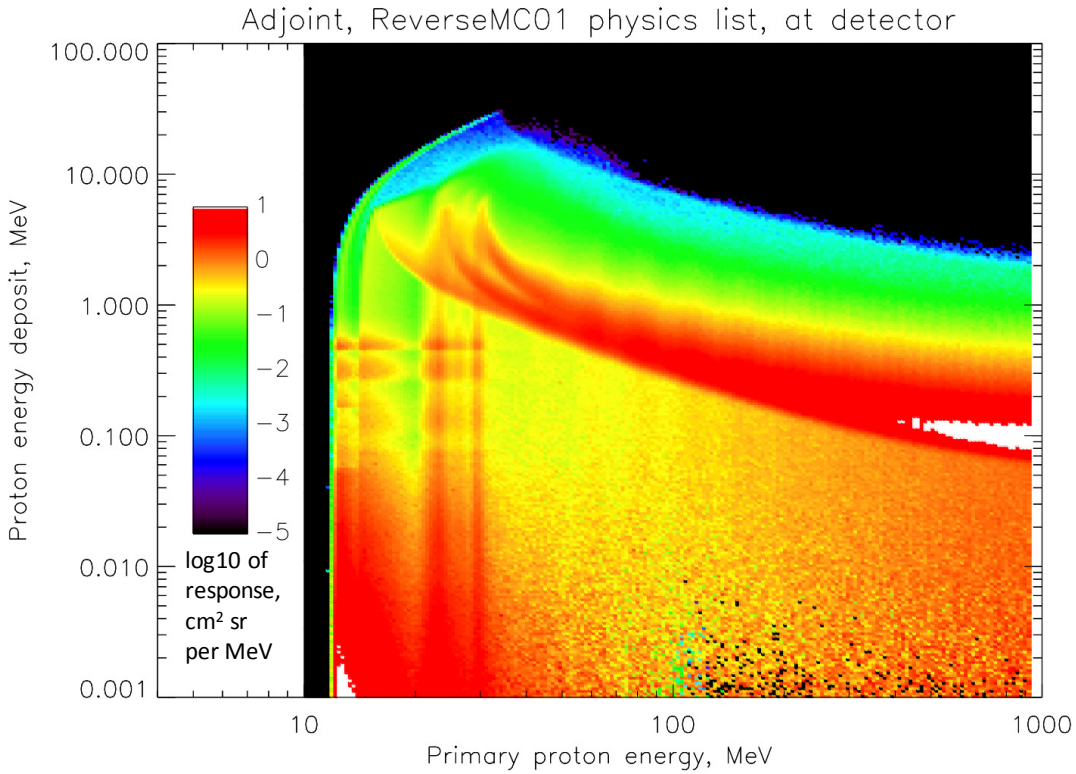

Figure 10. Same as Figure 9, but only tabulating energy deposits from protons at the adjoint source (surface of detector). Same colorscale as Figure 6.

Another way to compare the proton simulations is to tabulate the energy spectra of protons reaching the location of the adjoint source surface sphere as a function of primary proton energy. The color bars in the next few plots give the logarithm of this quantity in cm^2 sr per MeV (of penetrating proton energy, rather than of energy deposit as in Figures 6–10). Figure 11 shows the results for the forward simulation with Shielding_EMZ physics list, and Figure 12 is for the forward simulation with ReverseMC01 physics list. As with Figures 6 and 7, these two are very similar, except that Figure 12 is missing the spray of lower-energy penetrating protons produced by high-energy primary protons that lose some energy to nuclear interactions not in the ReverseMC01 physics list. By contrast, Figure 13 for the adjoint simulation (with adjoint source on the sphere to match Figures 11 and 12, not on the detector surface) shows a great enhancement of lower-energy protons reaching the sphere, including peculiar horizontal bands and a substantial strengthening of the vertical bands due to particles stopping in the detector.

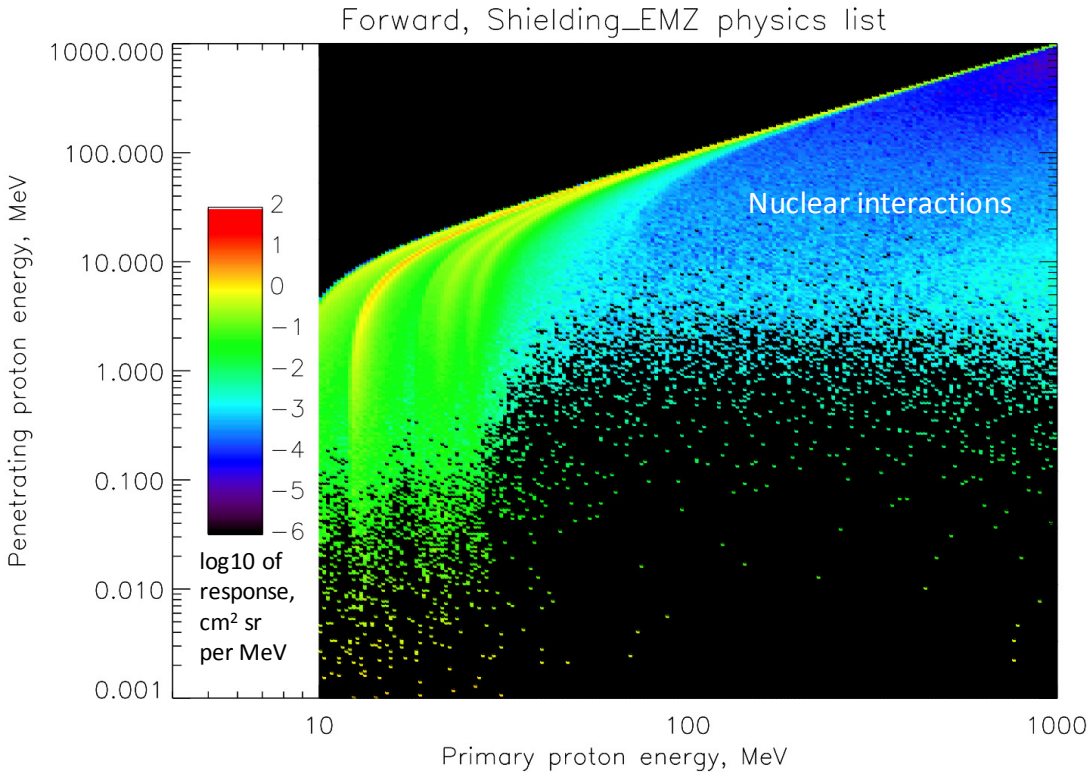

Figure 11. Spectra of protons reaching the adjoint source surface sphere plotted against primary proton energy, for the forward simulation with Shielding_EMZ physics list. Colorscale is logarithm of response in cm^2 sr per MeV of penetrating proton energy.

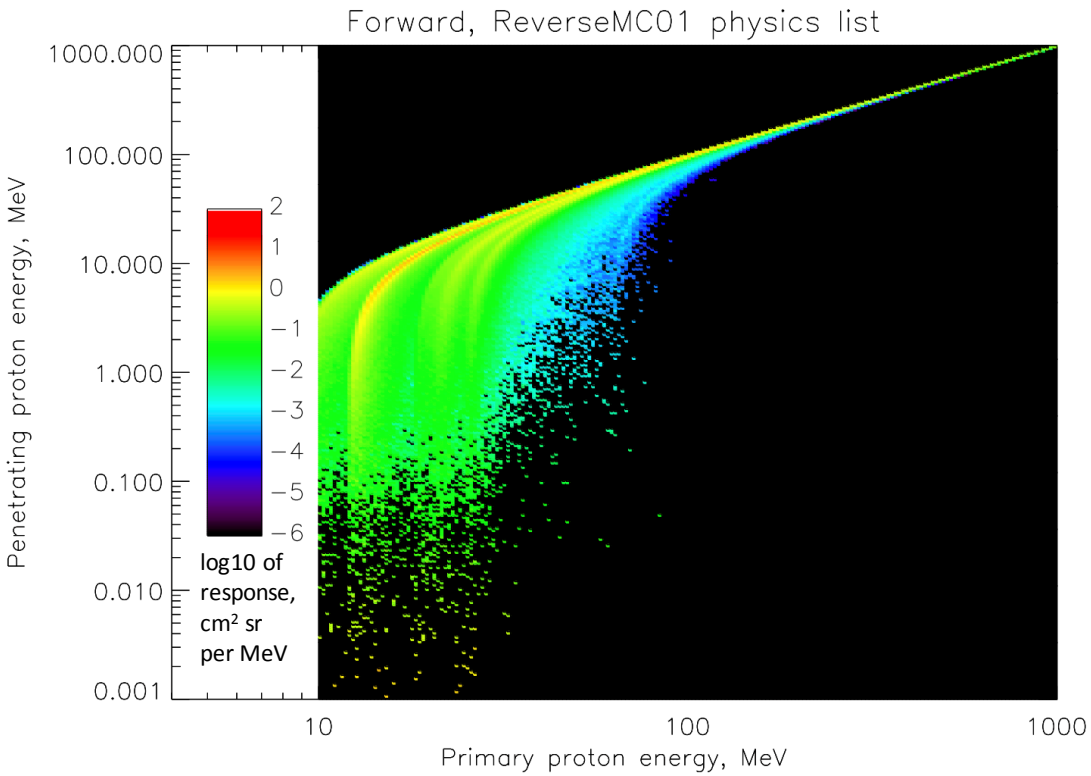

Figure 12. Spectra of protons reaching the adjoint source surface sphere plotted against primary proton energy, for the forward simulation with ReverseMC01 physics list. Same colorscale as Figure 11.

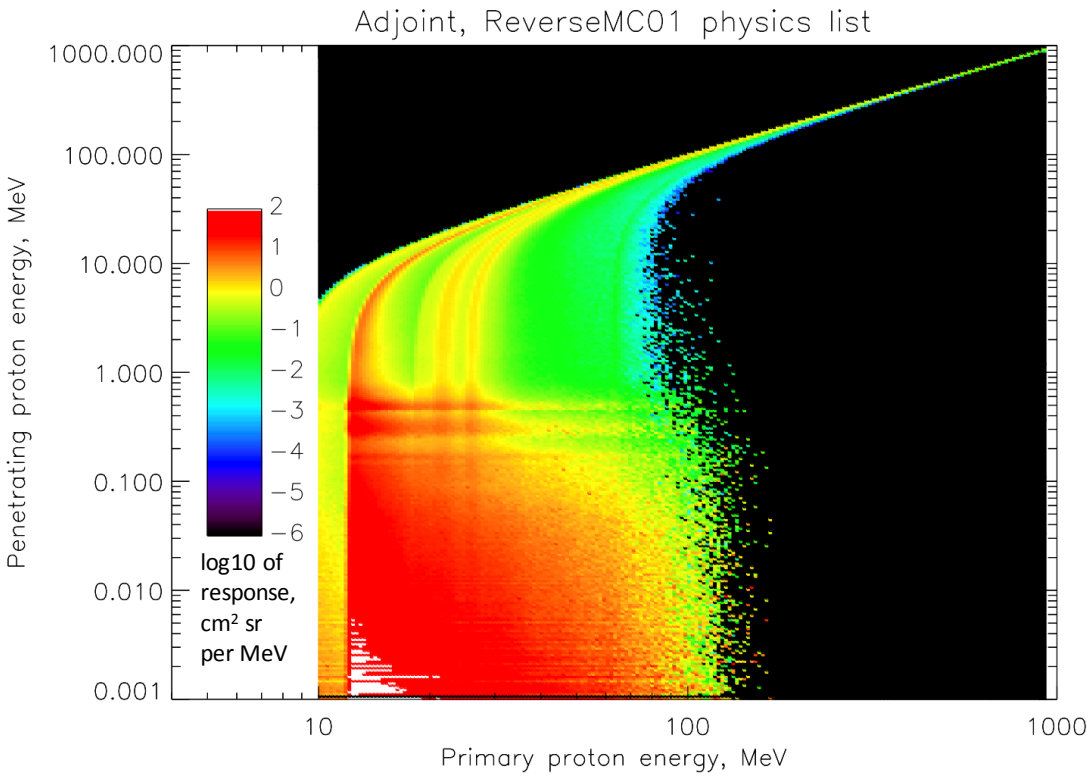

Figure 13. Spectra of protons reaching the adjoint source surface sphere plotted against primary proton energy, for the adjoint simulation with Shielding EMZ physics list. Same colorscale as Figure 11.

6. Combining Adjoint and Forward Simulations

We have also performed further comparisons between adjoint and forward Monte Carlo simulations of a microdosimeter in a realistic representation of its mounting in an actual spacecraft, to be reported separately, but the results for electrons herein (and comparisons of plots like those in Figures 6–13 for electrons, not shown) give us confidence that we can obtain accurate results from adjoint simulations of electrons. With regard to adjoint simulations of protons, we need to consider how to get around the apparent extra energy deposit and penetrating particle flux for lower-energy external primary protons that is evident in Figures 5, 8–10, and 13.

We have in the past spliced together separate forward simulations of the same geometry, with one simulation illuminating the area near the aperture of a sensor and the other illuminating the entire simulation geometry (e.g., Reference [2]). This allows us to model the complete background response of the sensor from all directions, while modeling the particles striking in and near the aperture with greater statistics to boost knowledge of the energy and angular distribution of the foreground response. Since the adjoint code provides information on the energy, position, and direction of the external primary particles corresponding to adjoint tracks that reach the outside of the simulation geometry, we can perform the same splicing of a focused forward simulation and a global adjoint simulation. We can combine forward simulations focused near the aperture of a sensor or the thinnest part of the shielding around a sensitive part with adjoint simulations that, implicitly, sample the whole geometry, simply cutting out the parts of the latter that correspond to the energies, positions, and/or angles sampled by the former. Since the adjoint simulations for protons appear to be most accurate at higher primary proton energies, and since these are the ones that would contribute to the omnidirectional background through the thicker portions of the shielding away from an aperture, this would allow us to avoid using the more dubious adjoint results for lower-energy external protons that stop in the sensitive volume. We are in the process of evaluating this combination procedure for the same realistic microdosimeter simulation mentioned above.

Another way to improve accuracy in the simulation results would be to use a more complete physics list, like Shielding_EMZ, for the forward transport of particles inward from the adjoint simulation source surface. This would, for example, enable tabulation of the larger energy deposits due to protons causing nuclear showers in the portions of the Kovar panels inside the green circle (sphere) in Figure 3, once those protons are found by the adjoint transport step to have been able to reach that volume from the outside of the simulation geometry. This would require a custom physics list combining the forward part (i.e., all) of a physics list like Shielding_EMZ with the adjoint part of ReverseMC01, and we have not had time to implement and test such a merged physics list. However, it would not address the apparent excess of lower-energy protons (or excess weight attached to them) from the adjoint transport step, as in Figure 13.

7. Improved Sector Shielding Calculation as an Alternative to Adjoint Proton Simulation

Another alternative to a forward Monte Carlo simulation that provides results with less computational effort is a deterministic sector shielding calculation. An energetic charged particle will lose approximately the same amount of energy to ionization when traversing a given column mass density (pathlength times volume mass density, measured in g/cm^2) through any material. Thus the amount of inert material over an electronic part, for example, may be represented for a shielding calculation as a thickness of a standard material, typically aluminum, with a column mass density equal to the sum of the column mass densities of the actual materials over it; the radiation dose in the part in a given external environment can then be approximated by looking up the result of a separate calculation of the dose under that depth of aluminum shielding. A more sophisticated calculation replaces this single representative equivalent thickness of aluminum with an integration over the equivalent thicknesses in all directions around the location of the part, as at left in Figure 14; this is called the sector shielding technique. A large sample of rays (green) are traced out in all directions from the location of the sensitive part, each one representing a fraction (sector) of the solid angle from which the geometry is illuminated, and for each one the column mass density along all segments of those rays traversing shielding material (yellow) are summed up. For each ray, the dose under the equivalent thickness of aluminum is calculated, and these doses are weighted by the solid angle represented by each single ray and integrated over all directions to give a total dose. Geant4 provides an easy means to perform such calculations, with an artificial "geantino" particle that is simply tracked in a straight line without scattering, energy loss, or other interactions of any kind; the pathlength through each element of the geometry can be summed up for each of many geantinos launched from the point of interest. This works better for protons than for electrons because they scatter less as they travel, so that the rays are a better approximation of their actual paths, but per section 5 we are most interested in this technique as an alternative to adjoint simulations of protons anyway and so we only discuss protons hereinafter.

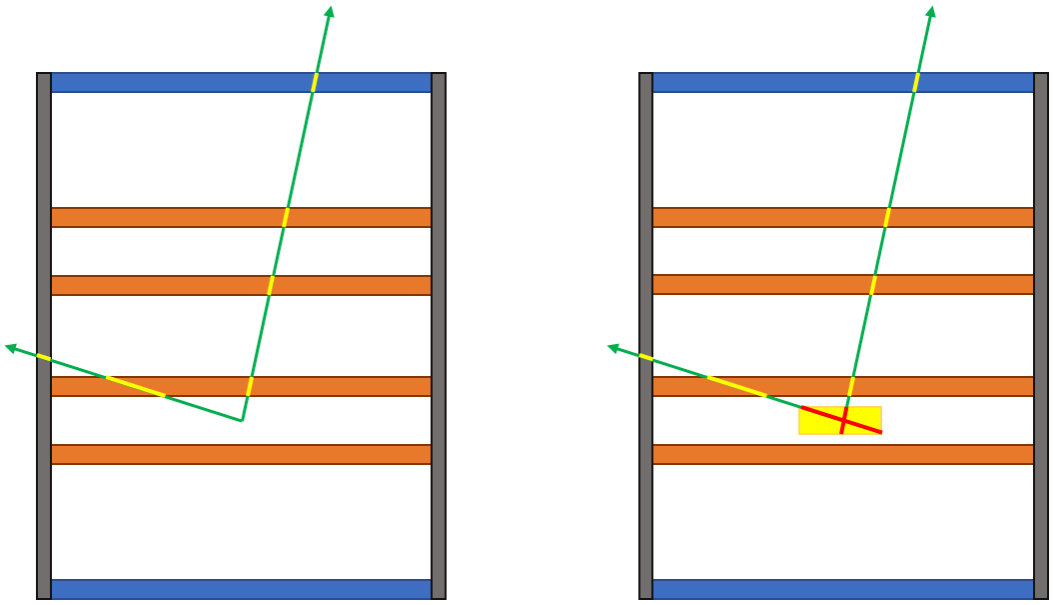

Figure 14. Schematic diagrams of pathlengths through shielding along rays outward from the location of a sensitive target for a sector shielding calculation (yellow segments of green rays) and, at right, along continuations of those rays through a finite volume of target material (red segments).

The tabulation of dose vs. shielding thickness used to obtain the contribution along each ray will typically give a single value of dose for a given external particle energy or energy spectrum, which represents an average (sum) over all pathlengths through the detector. We have developed an improvement to this calculation as shown at right in Figure 14, which enables us to calculate the distribution of individual energy deposits in the sensitive volume. This will make no difference to a simple dose calculation, provided that the geometry assumed in the tabulation of dose vs. shielding thickness is sufficiently representative of the actual geometry of interest (for example, the standard SHIELDOSE code provides options for dose at the center of an aluminum sphere, behind a flat slab of shielding, or between a flat slab of shielding and a semi-infinite backplane of aluminum). However, for problems that require information about the distribution of individual energy deposits, for example an electronic microdosimeter that only records dose deposited in pulses that are above a certain threshold, this improved technique provides this information; it also avoids the question of whether the geometry assumed in the dose vs. thickness tabulation is representative of the geometry of interest, since the actual configuration of the detector and shielding are used directly.

To perform this improved calculation, we use geantinos to trace rays outward through the geometry not from a single representative point of interest, but from origins uniformly and isotropically distributed over the surface of the sensitive volume, as represented by the green arrows in the right half of Figure 14. For each ray we also calculate the pathlength through the sensitive volume of the continuation (red lines) of each ray; therefore for each direction we have not just a column mass density of shielding but also a (maximum) pathlength through the sensitive volume for particles arriving along that direction from the outside of the simulation volume. For external particles of a given energy and arrival ray (position and direction), then, we calculate the energy deposit in the sensitive volume using a tabulation of particle ranges. We obtain this for protons from the online NIST PSTAR tool (http://physics.nist.gov/PhysRefData/Star/Text/PSTAR.html).

Figure 15 shows the values of range (in column mass density) vs. proton energy in materials representative of the test geometry in Figure 3 (Kovar is mostly iron and Mallory is mostly tungsten); the derivative of these curves gives the energy loss per unit column mass density, so that the similar slopes of the curves across much of the graph bear out the assertion that this quantity is approximately independent of the material. "CSDA" is the "continuous slowing-down approximation," which ignores fluctuations in the rate of energy loss and also ignores the effects of scattering in producing deviations from a straight-line trajectory; again, this deterministic approximation is better for protons than for electrons. For a given ray (position and direction), then, we have a summed column mass density of shielding σ_{sh} outside the sensitive volume and a geometric pathlength (also converted to a column mass density σ_{det}) of the continuation of that ray through the sensitive volume. For each external proton energy of interest E_{ext}, we determine the energy deposit E_{dep} in the sensitive volume as follows:

1. Calculate the range σ_{ext} in aluminum for a proton of energy E_{ext} from Figure 15.

2. Discard the proton if $\sigma_{sh} \geq \sigma_{ext}$. If not, $\sigma_{res\ Al} = \sigma_{ext} - \sigma_{sh}$ is the residual range in aluminum after penetrating the shielding.

3. Convert range $\sigma_{res\ Al}$ back to an energy E_{res}, representing the residual energy at the surface of the sensitive volume, using the aluminum curve in Figure 15.

4. Use the silicon curve in Figure 15 to convert E_{res} to the remaining range $\sigma_{res\ Si}$ in the sensitive volume.

5. If $\sigma_{res\ Si} \leq \sigma_{det}$, the $E_{dep} = E_{res}$. Otherwise, $\sigma_{esc} = \sigma_{res\ Si} - \sigma_{det}$ is the residual range of the proton escaping through the sensitive volume.

6. Use the silicon curve in Figure 15 to convert σ_{esc} to the energy E_{esc} of the escaping proton, and $E_{dep} = E_{res} - E_{esc}$.

These are essentially the same steps as in a forward Monte Carlo calculation, though with all scattering, interactions, fluctuations, etc. replaced by a deterministic range-energy calculation and only trajectories striking the detector considered; thus the results should be directly comparable.

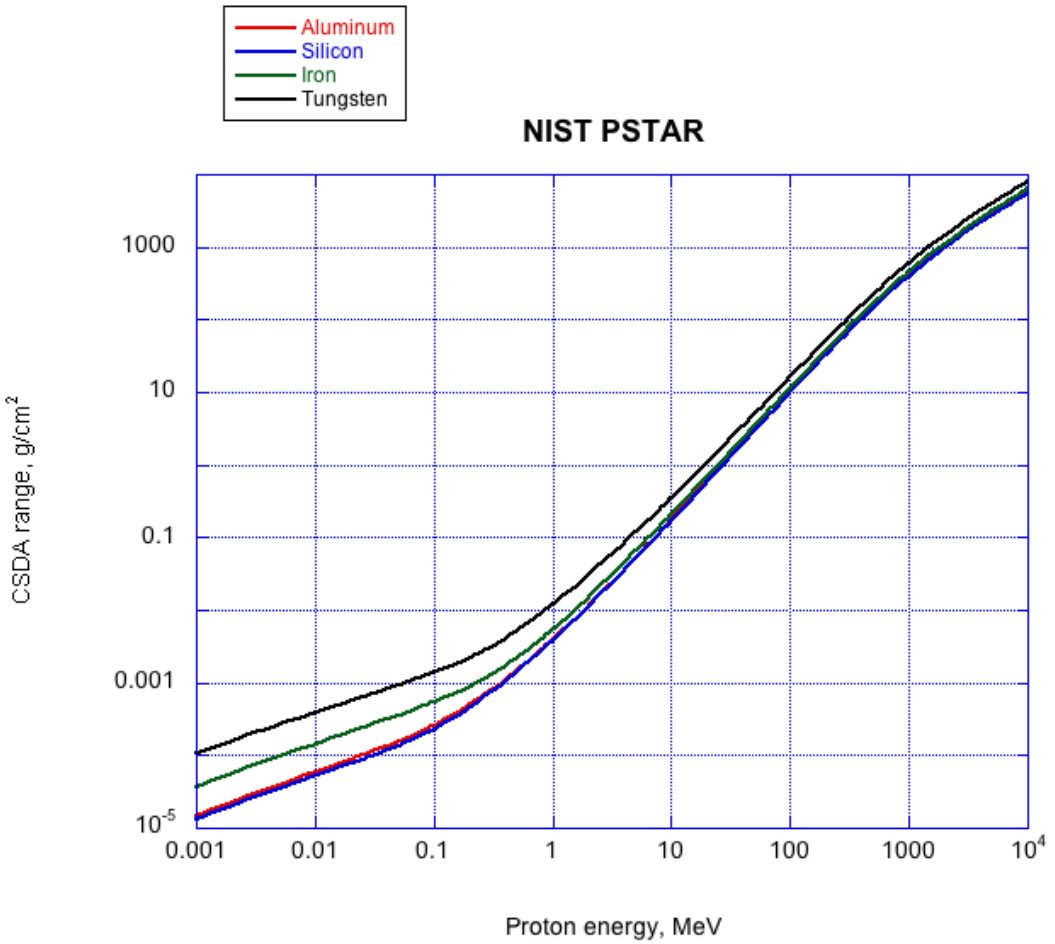

Figure 15. Range vs. energy for protons in various materials, from NIST PSTAR tabulation.

Figure 16 shows the dose response calculated by this means as the blue curve with "Al CSDA" in parentheses as part of the legend; the red curve is the result of the forward Monte Carlo simulation with ReverseMC01 physics list as in Figure 5 (same as the blue curve in that figure). The overall normalization and general shape agree very well between the two curves, but the sector shielding calculation is systematically shifted toward higher energies, which could be a problem when convolving this result with a steeply falling external proton spectrum. The energy shift is the result of the limits of the approximation that energy deposit per unit column mass density is the same for all materials; for example, the ranges plotted in Figure 15 show that a proton of 11.4 MeV could make it through the 10 mils of Mallory (represented as tungsten) that represent the thinnest shielding around the detector in the test geometry in Figure 3, but that it would take 16.9 MeV for a proton to penetrate the same column mass density of aluminum, so that the dose from protons penetrating this wall is shifted to higher energies. The different humps and shoulders in the curves in Figure 16 represent subsets of the protons penetrating through different parts of the geometry; thus we can tune the thresholds by relating range through shielding to a column density of a different baseline material, say iron rather than aluminum to obtain the green curve in Figure 16. This does line up one shoulder, representing paths that travel mostly through Kovar in the test geometry, but reproducing the entire forward Monte Carlo curve is not possible when relating heterogenous materials to a single baseline via their column mass densities.

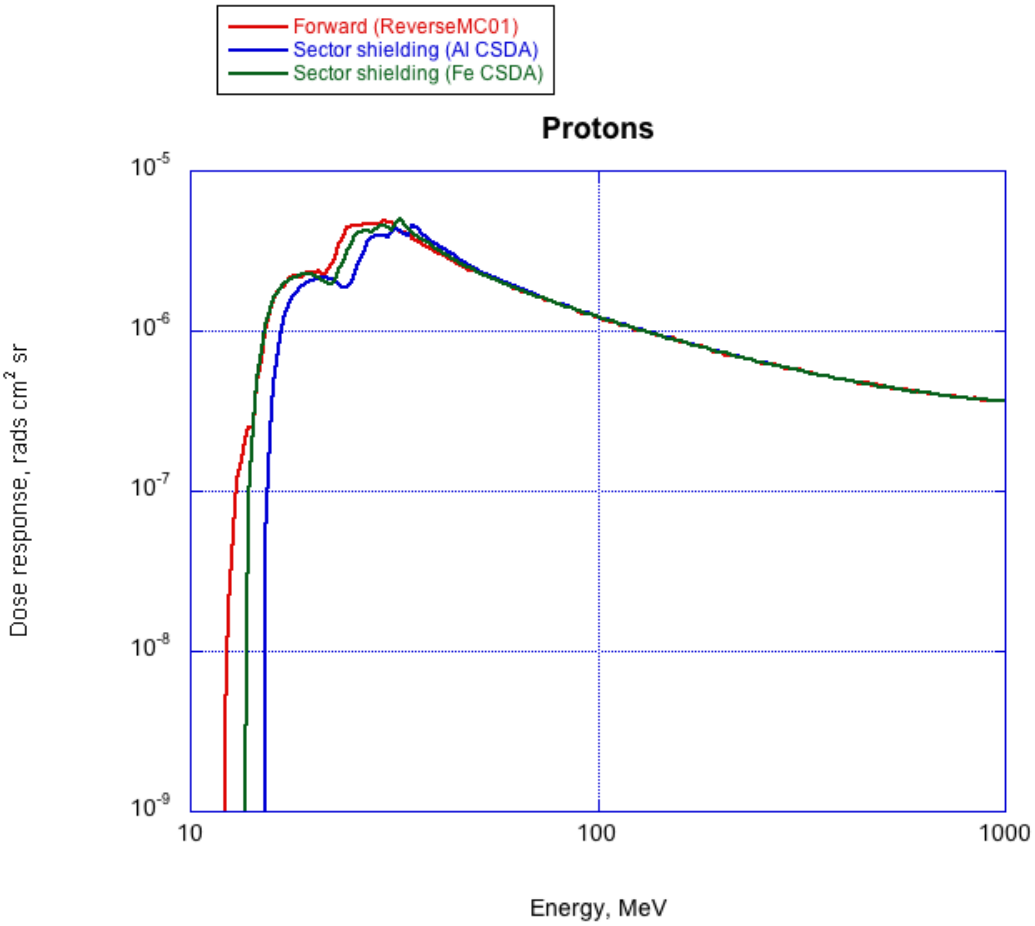

Figure 16. Dose response for protons in the test geometry from a forward Monte Carlo simulation and from two different scalings of the sector shielding calculation.

A further improvement in this technique results when we scale the column mass densities that are summed up inside different materials along each ray, introducing a correction for the differences between

the curves in Figure 15. Since the ratio between values in these curves varies with energy whereas each ray calculation is intended to apply to all energies, this will not be perfect; however, here we choose values around 100 MeV, as the typical energy range for penetration of the geometry, dividing the geantino-sampled column mass densities by 0.98, 1.15, and 1.6 for silicon, Kovar, and Mallory respectively to better represent the equivalent column mass densities in aluminum. The results of this calculation are shown in Figure 17, and it is clear that agreement with the forward Monte Carlo calculation is greatly improved.

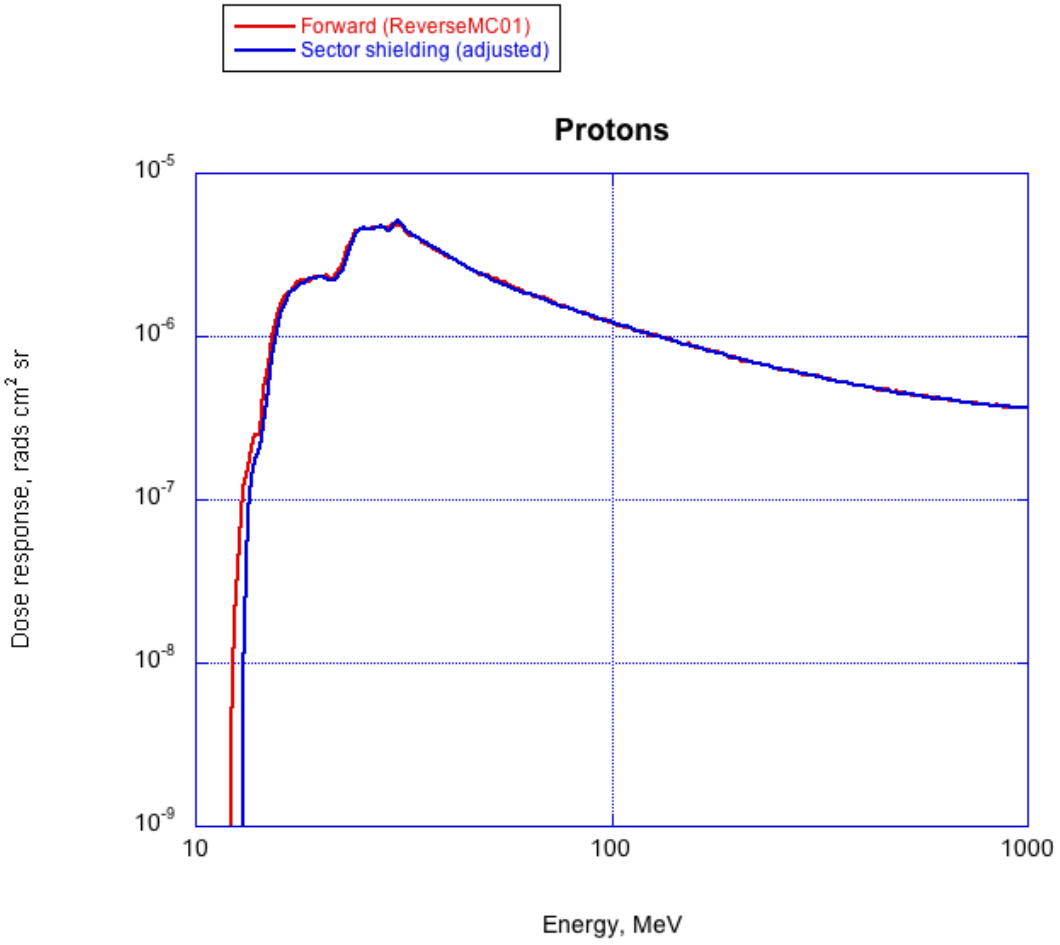

Figure 17. Dose response for density-adjusted sector shielding calculation compared with forward Monte Carlo result.

As noted above, the tabulation of actual pathlengths in the target sensitive volume allows for calculation of individual (rather than just average) energy deposits, so we can display this quantity as in Figure 18, for direct comparison with the result of the forward Monte Carlo calculation in Figure 7. Scattering and energy-deposit fluctuations in the Monte Carlo simulation spread out the various structures due to families of trajectories through particular combinations of shielding elements, and the CSDA sector shielding calculation of course entirely omits the broad patch of low energy deposits due to secondary electrons that strike the detector even when the primary proton misses (*cf.* the difference between Figures 9 and 10). However, as is clear from Figure 17, the vast majority of the energy deposit is shown in the correct places by this much simpler calculation, and thus we conclude that our modified sector shielding technique is a good substitute for the adjoint proton Monte Carlo calculations with which we had difficulty as explained in section 5.

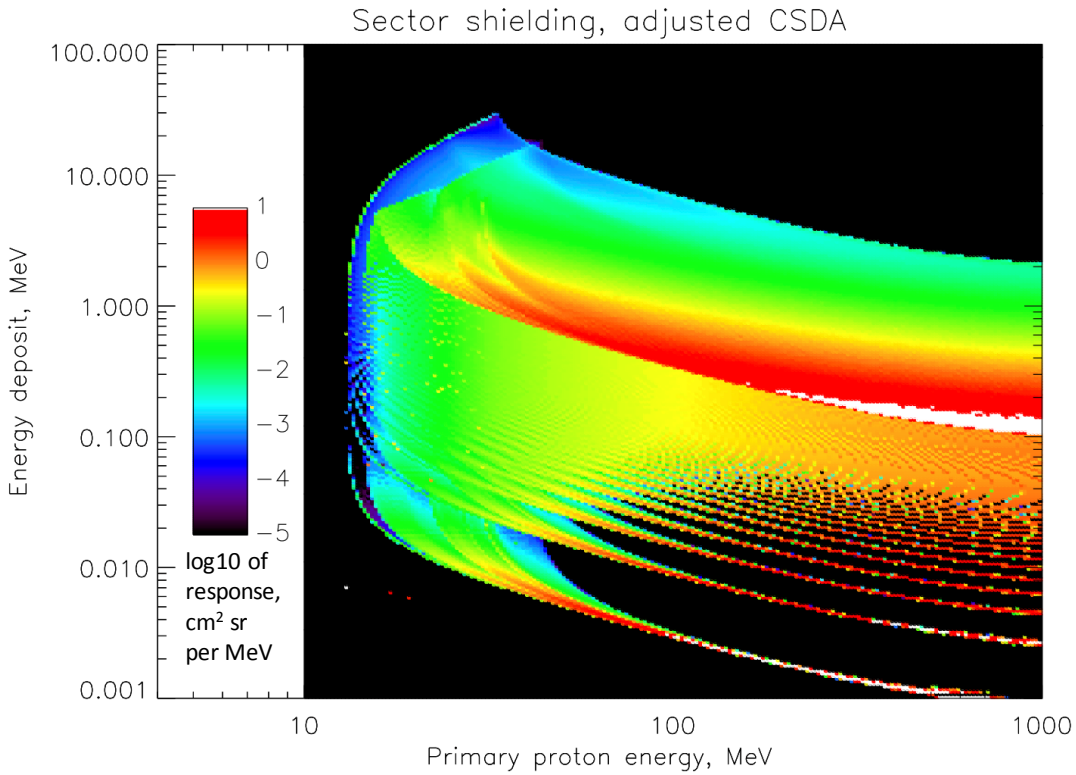

Figure 18. Spectra of energy deposits in detector as a function of primary proton energy, for sector shielding calculation with CSDA ranges adjusted per material. Same colorscale as Figure 6.

8. Summary

We have presented here a discussion of alternatives to the standard forward Monte Carlo simulations enabled by the Geant4 radiation-transport toolkit, and a comparison of the results of these different modeling techniques in a simple test geometry. These alternatives provide faster results, in particular, for calculations of radiation dose to small sensitive volumes inside a large geometry of inert shielding material, at the cost of some reduction in the realism of the details of the simulated physics.

In the space radiation environment, especially that due to trapped radiation in the Earth's magnetosphere, the primary particle species of interest are electrons and protons. For electrons, we find that the adjoint Monte Carlo technique, as implemented in recent versions of Geant4 (version geant4.10.03.p02 is considered here), gives results for dose vs. primary electron energy that are in good agreement with those from the well-established forward Monte Carlo technique in the same code.

For protons, we find that the adjoint technique produces substantial and unrealistic enhancements of dose for particles that come to a stop, or nearly, in the sensitive detector. We can mitigate this by using the results of the adjoint simulation only for penetrating proton energies, replacing the problematic parts of the results with those from forward simulations focused on the thinner parts of the shielding, though we did not address this quantitatively in this report. We did, however, evaluate the even faster sector shielding technique for calculation of proton dose. We modified the standard version of this technique by (1) adjusting the tabulated column mass densities for different shielding materials to better represent their effects on slowing down the incident protons, and (2) calculating energy deposit along a realistic representation of pathlengths through the sensitive detector, rather than using a look-up table that averages over these pathlengths. With these modifications, the sector-shielding technique gives results for dose vs. primary proton energy that are in good agreement with those from the forward Monte Carlo technique.

9. References

1. Allison, J., *et al*. (2016), "Recent Developments in Geant4," *Nucl. Instrum. Methods Phys. Res. A* **835**, 186-225, doi: 10.1016/j.nima.2016.06.125

2. Looper, Mark (2016), *Updated Geant4 Simulations of AeroCube 6 Microdosimeters*, TOR-2016-03260.

3. Looper, M. D., et al. (2013), "The Radiation Environment Near the Lunar Surface: CRaTER Observations and Geant4 Simulations," *Space Weather* **11** (4), 142-152, doi: 10.1002/swe.20034

4. O'Brien, T. P.; J. E. Mazur; T. B. Guild; and M. D. Looper (2015), "Using Polar-orbiting Environmental Satellite Data to Specify the Radiation Environment up to 1200 km Altitude," *Space Weather* **13**, 433-445, doi: 10.1002/2015SW001166

Appendix A. Notes on the Adjoint Code

The adjoint simulation example code ReverseMC01 includes RMC01AnalysisManager.cc, which centralizes the scoring routines for the example. The example can be run in either forward or adjoint mode; this appendix presents some notes on how to extract information on all the results of an adjoint Monte Carlo simulation. The values used to prepare the analyses in this report were dumped to an ASCII file by a modified version of

```
void RMC01AnalysisManager::EndOfEventForAdjointSimulation(const G4Event* anEvent)
```

which is invoked after successful transport of one initial adjoint particle (electron, gamma, or proton). That is, as discussed in section 2, each full adjoint cycle includes the launching of up to three initial adjoint particles of different species, and the above method is invoked whenever any one of the three has been transported backward in time, found to have been caused by a valid external primary particle, and then transported forward in time through the sensitive volume.

The scoring results from the forward transport inside the sensitive volume, such as the energy deposit from the electrons, gammas, or protons therein, are accessible in the same way as in a standard forward simulation, so no details will be given here. The initial ("primary" in Geant4 terminology, as noted in section 2) adjoint particle that has just been processed is accessible through

```
G4PrimaryVertex* pv = anEvent->GetPrimaryVertex();
G4PrimaryParticle* pp = pv->GetPrimaryParticle();
```

The species, position, energy, and direction of this particle, as well as other properties, are accessible through various methods of G4PrimaryParticle and G4PrimaryVertex. Access to the properties of the tracks produced by the adjoint transport stage is through

```
G4AdjointSimManager* theAdjointSimManager = G4AdjointSimManger::GetInstance();
size_t nt = theAdjointSimManger->GetNbOfAdjointTracksReachingTheExternalSurface();
```

"nt" is the number of adjoint tracks for the given initial adjoint particle that reach the outside of the simulation volume, possibly with different species when they reach that outside surface; all must be tabulated to fully account for the results of the adjoint simulation. (Of course, if one is only interested in protons as external primary particles, for example, then one can discard any tracks that don't reach the outer surface as protons.) The properties of each of the tracks, with index j = 0 to nb – 1, are obtained with methods like

```
G4double prim_ekin = theAdjointSimManager->GetEkinAtEndOfLastAdjointTrack(j);
G4double adj_weight = theAdjointSimManager->GetWeightAtEndOfLastAdjointTrack(j);
G4ThreeVector prim_pos = theAdjointSimManager->GetPositionAtEndOfLastAdjointTrack(j);
```

and so on. As it happens,

```
G4String p_name = theAdjointSimManager->GetFwdParticleNameAtEndOfLastAdjointTrack();
```

is not indexed, so it only returns the name of the last (number j = nt – 1) track. To identify the species of each track j, use

```
G4int pdg = theAdjointSimManager-
>GetFwdParticlePDGEncodingAtEndOfLastAdjointTrack(j);
```

to get the Particle Data Group number for the external primary particle, and compare it with

```
G4int pdg_e = G4Electron::Electron()->GetPDGEncoding();
```

etc.

Finally, the adjoint transport step was first enabled to produce multiple tracks for a single initial adjoint particle in version 10.3 of Geant4; in earlier versions, only one track was traced outward for each initial adjoint particle. To check if the strange results discussed in section 5 were somehow due to our mishandling the multiple adjoint tracks in version 10.3, we redid the adjoint simulations with version 10.2 of Geant4. The proton results were essentially identical to those in Figure 5 and section 5, so this was not the case; we also found that the electron dose response curve in Figure 4 was about 20% below the green adjoint curve for version 10.3. Thus version 10.3 is an improvement for electrons, and doesn't change proton results; and we confirm that we are adding contributions from the multiple adjoint tracks correctly.

External Distribution

REPORT TITLE

Adjoint Monte Carlo Simulations and Improved Sector Shielding Calculations with Geant4

REPORT NO.	PUBLICATION DATE	SECURITY CLASSIFICATION
ATR-2018-00052	March 12, 2018	UNCLASSIFIED

Capt. Felix A. Abeyta
USAF
felix.abeyta.1@us.af.mil

Makoto Asai
Stanford Linear Accelerator Center
asai@slac.stanford.edu

Robin J. Barnes
Johns Hopkins University
Applied Physics Laboratory
Robin.Barnes@jhuapl.edu

Laurent Desorgher
Centre Hospitalier Universitaire Vaudois
Laurent.Desorgher@chuv.ch

Michael A. Kelly
Johns Hopkins University
Applied Physics Laboratory
Michael.Kelly@jhuapl.edu

Tom Sotirelis
Johns Hopkins University
Applied Physics Laboratory
Tom.Sotirelis@jhuapl.edu

Insoo Jun
JPL
insoo.jun@jpl.nasa.gov

Release to Public	Control Export
Yes ☑ No ☐	Yes ☐ No ☑

APPROVED BY_____ DATE_____
(AF OFFICE)

AEROSPACE REPORT NO.
ATR-2018-00052

Adjoint Monte Carlo Simulations and Improved Sector Shielding Calculations with Geant4

Approved Electronically by:

James L. Roeder,
DIRECTOR
SPACE SCIENCES
DEPARTMENT
SPACE SCIENCE
APPLICATIONS
LABORATORY
ENGINEERING &
TECHNOLOGY GROUP

James H. Clemmons, PRINC
DIRECTOR
SPACE SCIENCE
APPLICATIONS
LABORATORY
PHYSICAL SCIENCES
LABORATORIES
ENGINEERING &
TECHNOLOGY GROUP

Lynn M. Friesen, PRINC
DIRECTOR
OFFICE OF PRODUCT
MANAGEMENT
TECHNOLOGY &
LABORATORY
OPERATIONS
ENGINEERING &
TECHNOLOGY GROUP

Cognizant Program Manager Approval:

Margaret W. Chen, ASSOC DIRECTOR
SPACE SCIENCES DEPARTMENT
SPACE SCIENCE APPLICATIONS LABORATORY
ENGINEERING & TECHNOLOGY GROUP

Aerospace Corporate Officer Approval:

Charles L. Gustafson, SR VP ENG & TECH
ENGINEERING & TECHNOLOGY GROUP

SL0338

AEROSPACE REPORT NO.
ATR-2018-00052

Adjoint Monte Carlo Simulations and Improved Sector Shielding Calculations with Geant4

Content Concurrence Provided Electronically by:

Mark D. Looper, RES SCIENTIST
MAGNETOSPHERIC & HELIOSPHERIC SCIENCES
SPACE SCIENCES DEPARTMENT
ENGINEERING & TECHNOLOGY GROUP

Technical Peer Review Performed by:

T Paul O'Brien, RES SCIENTIST
AVIR MAGNETOSPHERIC & HELIOSPHERIC SCI
SPACE SCIENCES DEPARTMENT
ENGINEERING & TECHNOLOGY GROUP

Office of General Counsel Approval Granted Electronically by:

Domenic C. Rigoglioso, ASSOC GEN COUNSEL
OFFICE OF THE GENERAL COUNSEL
OFFICE OF GENERAL COUNSEL & SECRETARY

Export Control Office Approval Granted Electronically by:

Edward Pevzner, EXPORT CONTROL STAFF IV
GOVERNMENT SECURITY
SECURITY OPERATIONS
OPERATIONS & SUPPORT GROUP

SL0338